Quasiparticle and optical properties of polythiophene-derived polymers

Georgy Samsonidze,* Filipe J. Ribeiro,† Marvin L. Cohen, and Steven G. Louie
Department of Physics, University of California, Berkeley, California 94720, USA
and Materials Sciences Division, Lawrence Berkeley National Laboratory, Berkeley, California 94720, USA

(Received 10 March 2014; revised manuscript received 3 July 2014; published 17 July 2014)

Electron donor conjugated polymers blended with electron acceptor fullerene derivatives is one of the promising technologies for organic photovoltaics. However, with the energy conversion efficiency of only 9% in a single bulk heterojunction device structure, these solar cells are not yet competitive with conventional inorganic semiconductor technology. Some of the limitations are large optical band gaps and small electron affinities of polymers preventing the absorption of infrared radiation and leading to energy losses during charge separation at the donor-acceptor interface, respectively. In this work, we compute from first principles the quasiparticle and optical spectra of several different thiophene-, ethyne-, and vinylene-based copolymers using the GW method and the GW plus Bethe-Salpeter equation approach. One of the polymers is identified which has a preferential alignment of the energy levels at the interface with fullerene molecule compared to the reference case of polythiophene.

DOI: 10.1103/PhysRevB.90.035123 PACS number(s): 71.20.Rv, 71.20.Tx, 78.40.Me, 78.40.Ri

I. INTRODUCTION

Bulk heterojunction (BHJ) blends of conjugated polymers and fullerene derivatives are among the highest-efficiency organic photovoltaic (OPV) cells [1]. Energy conversion efficiencies in the range of 4.4% to 6.1% have been reported for single BHJ blends composed of electron donor poly(3-hexylthiophene) (P3HT) polymers and electron acceptor [6,6]-phenyl-C_{61} butyric acid methyl ester (PCBM) molecules [2–6]. P3HT and PCBM are derivatives of polythiophene (PT) polymers and buckminsterfullerene (C_{60}) molecules functionalized for aqueous solubility to enable solution processing. Further theoretical studies have shown that the energy conversion efficiency can be increased by replacing P3HT with another polymer which has a smaller optical band gap and a larger electron affinity compared to P3HT [7–9]. These conditions ensure minimal energy losses in the absorption of solar radiation and in the charge separation at the interface with PCBM molecules, respectively. There has been considerable activity in the synthesis of conjugated polymers with low optical band gaps, as well as in replacing the electron acceptor, for instance with [6,6]-phenyl-C_{71} butyric acid methyl ester ($PC_{71}BM$) molecules. The best energy conversion efficiencies for a single BHJ device have been 6.77% using PBDTTT:PCBM [10], 7.4% using PTB7:$PC_{71}BM$ [11], 8.37% using PTB7:PCBM [12], 7.4% using PDTG-TPD:$PC_{71}BM$ [13], 9.21% using PTB7:$PC_{71}BM$ [14], and 7.9% using PDTP-DFBT:$PC_{71}BM$ [15]. It should also be noted that the energetics of the interface is only one of the factors affecting the energy conversion efficiency, others being the mobility of the charge carriers and the morphology of the BHJ film [16–18].

This paper conducts a computational search for a conjugated polymer with the optical band gap and the electron affinity tuned for maximum performance in BHJ solar cells with PCBM molecules serving as electron acceptor. In Sec. II, the quasiparticle and optical spectra of several different thiophene-, ethyne-, and vinylene-based copolymers placed in a vacuum environment are calculated from first principles using the GW approximation to the electron self-energy and solving the Bethe-Salpeter equation (BSE) to include electron-hole interaction in the optical response. In Sec. III, the effects of the side chain substitution, the interface dipole layer, the hybridization of electronic orbitals of adjacent PCBM molecules, and the polarization of the BHJ blend are taken into account. In Sec. IV, the energetics of the interface between the polymers and PCBM molecules is analyzed and one of the polymers is identified which has lower energy losses compared to PT during both optical absorption and charge separation processes.

II. ISOLATED POLYMERS

Several copolymers made of two thiophene units and different combinations of ethyne, vinylene, or vinylene derivatives were investigated in this work. Quasiparticle band structures and optical absorption spectra of these polymers placed in a vacuum environment were calculated using *ab initio* electronic-structure methods based on density functional theory (DFT) for the ground state and many-body Green's function theory for excited state properties. Similar calculations were performed for the C_{60} molecule. The computational methodology is described below in details. Six polymers were selected which show a strong optical absorption in the near-infrared and red parts of the spectrum (0.8–2 eV). This range of values for the optical band gap gives minimal energy losses in the absorption of solar radiation [19]. Chemical names and abbreviations of the selected polymers along with C_{60} molecule are listed in the first two columns of Table I. The corresponding ball-and-stick models are shown in Fig. 1.

Our computational methodology consists of the following three steps: (i) The equilibrium atomic positions and the electronic ground state are obtained from DFT using the generalized gradient approximation (GGA) by Perdew-Burke-Ernzerhof (PBE) for the exchange-correlation potential

*Present address: Research and Technology Center, Robert Bosch LLC, Cambridge, Massachusetts 02142.
†Present address: Google Inc.

TABLE I. Results of the DFT, G_0W_0, and BSE calculations for isolated thiophene-based polymers, isolated C_{60} and PCBM molecules, and isolated polythiophene:C_{60} interface. E_v, E_c, and E_g represent the valence band maximum (VBM) or the highest occupied molecular orbital (HOMO), the conduction band minimum (CBM), or the lowest unoccupied molecular orbital (LUMO), and the quasiparticle band gap, respectively. The E_v and E_c values are relative to the vacuum level. E_o and E_b represent the optical excitation energy and the binding energy of the lowest bright exciton, respectively. The G_0W_0 and BSE columns summarize the data shown in Figs. 2 and 3, respectively. All energies are in eV.

Abbreviations and chemical names		DFT			G_0W_0			BSE	
		E_v	E_c	E_g	E_v	E_c	E_g	E_o	E_b
PT	polythiophene	−4.26	−3.21	1.05	−5.35	−2.25	3.10	1.48	1.62
PMeT	poly(methyl thiophene)	−3.94	−2.87	1.07	−4.98	−1.97	3.01	1.48	1.53
P3HT	poly(3-hexylthiophene)	−3.79	−2.80	0.99					
PDTE	poly(dithiophene ethyne)	−4.44	−3.36	1.08	−5.52	−2.39	3.13	1.79	1.34
PDTV	poly(dithiophene vinylene)	−4.19	−3.36	0.83	−5.14	−2.52	2.62	1.23	1.39
P3HDTV	poly(3-hexyldithiophene vinylene)	−3.81	−3.12	0.69					
PDTDCNV	poly(dithiophene dicyanovinylene)	−5.26	−4.63	0.63	−6.04	−3.86	2.18	1.00	1.18
PDTDFV	poly(dithiophene difluorovinylene)	−4.43	−3.46	0.97	−5.48	−2.54	2.94	1.45	1.49
PDTDCV	poly(dithiophene dichlorovinylene)	−4.53	−3.52	1.01	−5.58	−2.64	2.94	1.46	1.47
C_{60}	buckminsterfullerene	−5.84	−4.19	1.65	−7.31	−2.75	4.56	3.50	1.06
PCBM	[6,6]-phenyl-C_{61} butyric acid methyl ester	−5.43	−3.96	1.47					
PT:C_{60}	polythiophene:buckminsterfullerene	−4.49	−4.06	0.43					
PDTV:C_{60}	poly(dithiophene vinylene):buckminsterfullerene	−4.37	−4.08	0.29					

[20,21], the Troullier-Martins norm-conserving pseudopotentials [22] in the Kleinman-Bylander nonlocal separable form [23], and the plane-wave basis set. (ii) The quasiparticle band structure is calculated using the GW approximation to the electron self-energy within the generalized plasmon pole (GPP) model [24,25]. The electronic Green's function G and the dynamically screened Coulomb interaction W are constructed from the DFT Kohn-Sham orbitals and eigenvalues which is commonly referred as the G_0W_0 method. (iii) The macroscopic absorption spectrum is obtained by solving the Bethe-Salpeter equation using the Tamm-Dancoff approximation (decoupling resonant and antiresonant transitions) and ignoring dynamical properties of the screened Coulomb interaction [26,27]. The polarization of light is directed along the polymer backbone. Step (i) is performed using the PARATEC code [28], steps (ii) and (iii) using the BERKELEYGW package [29]. Additional computational details are given in the next paragraph.

The supercell method [30] was used throughout the calculations. The bare Coulomb potential used in G_0W_0 and BSE

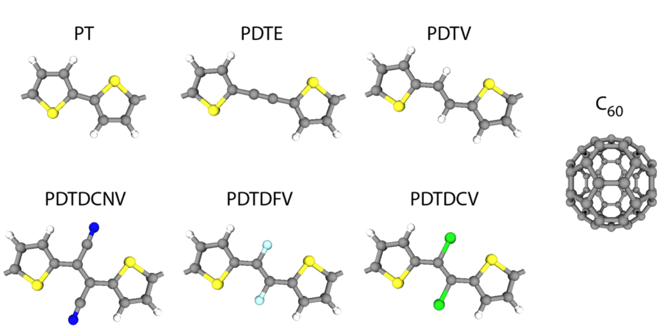

FIG. 1. (Color online) Ball-and-stick models of thiophene-based polymers and C_{60} molecule. Chemical names and abbreviations are listed in the first two columns of Table I. White, gray, blue, cyan, green, and yellow spheres represent hydrogen, carbon, nitrogen, fluorine, chlorine, and sulfur atoms, respectively.

calculations was truncated at the faces of the supercell in the nonperiodic directions (along the lattice vectors $\mathbf{a}_1$ and $\mathbf{a}_2$ for polymers or $\mathbf{a}_1$, $\mathbf{a}_2$, and $\mathbf{a}_3$ for the C_{60} molecule) to avoid spurious interactions between periodic replicas of the system [31]. To retain the Coulomb interaction within the system, the size of the supercell in the nonperiodic directions was set to twice the size of the box confining the isosurface that encloses 99% of the electron density [32]. The DFT Kohn-Sham eigenvalues were referred to the vacuum level obtained by averaging the electrostatic (ionic plus Hartree) potential at the faces of the supercell in the nonperiodic directions. The kinetic energy cutoff for the plane-wave expansion of the Kohn-Sham orbitals and the bare Coulomb potential was set to 51–82 Ry (depending on the elements in the polymer), while 6 Ry was used for the dielectric function and the screened Coulomb potential. Atomic positions were relaxed to equilibrium using thresholds of 10^{-4} Ry/bohr and 10^{-5} Ry/bohr^3 on forces and stresses, respectively.

In the DFT and G_0W_0 calculations, the Brillouin zone (BZ) was sampled using a shifted Monkhorst-Pack [33] coarse grid of size $1\times1\times16$ for PT, while $1\times1\times12$ coarse grid was used for other polymers (because of their larger unit cells compared to PT) and the Γ point for the C_{60} molecule. In the BSE calculations, $1\times1\times64$ and $1\times1\times48$ shifted fine grids and the Γ point were used, respectively. To accelerate the convergence of G_0W_0 and BSE calculations with the number of $\mathbf{k}$ points, the Coulomb potential was averaged inside the Voronoi cell around the Γ point [29]. In the G_0W_0 calculations, the static irreducible polarizability in the random phase approximation (RPA) and the electron self-energy were computed by summing over 1592–2578 unoccupied orbitals with eigenvalues up to 6 Ry above the vacuum level for different polymers, while 5370 unoccupied orbitals up to 3 Ry above the vacuum level were used for the C_{60} molecule. To accelerate the convergence of the self-energy with the number of unoccupied orbitals, the static remainder correction was applied [34]. Using the

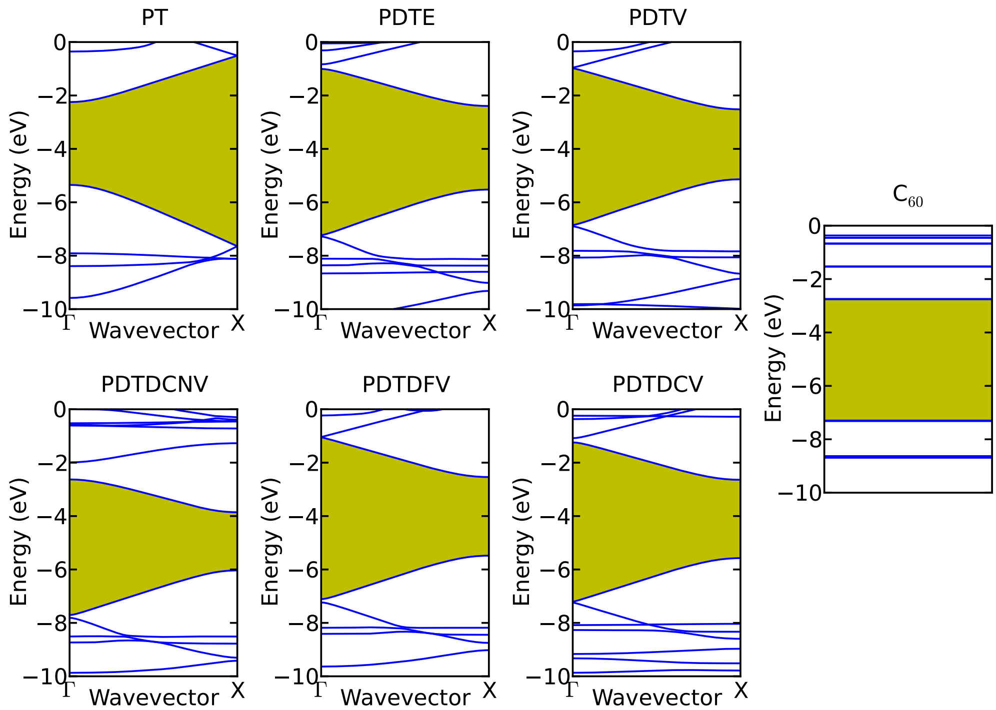

FIG. 2. (Color online) Quasiparticle band structures of isolated thiophene-based polymers and quasiparticle energy levels of isolated C_{60} molecule calculated using the G_0W_0 method within the generalized plasmon pole (GPP) model. Chemical names and abbreviations are listed in the first two columns of Table I. The band gaps are shaded in yellow. The zero reference for the energy scale is the vacuum level.

aforementioned numbers of unoccupied orbitals without the static remainder correction gives convergence errors in the self-energy of about 0.2 eV for polymers and 0.5 eV for the C_{60} molecule. In the BSE calculations, the electron-hole interaction kernel was computed on the coarse **k** grid between the occupied and unoccupied orbitals within the range of 4 eV from the valence and conduction band edges and then interpolated to the fine **k** grid. The 4-eV energy range includes 8 occupied and 8 unoccupied orbitals for polymers or 31 occupied and 54 unoccupied orbitals for the C_{60} molecule.

The results of our calculations are summarized in Table I and in Figs. 2 and 3. DFT Kohn-Sham eigenvalues of the valence band maximum (VBM) and the conduction band minimum (CBM) of the polymers or the highest occupied molecular orbital (HOMO) and the lowest unoccupied molecular orbital (LUMO) of the C_{60} molecule are listed in Table I in the columns labeled E_v and E_c, respectively, under the "DFT" heading. DFT Kohn-Sham band gaps $E_g = E_c - E_v$ are also shown in Table I. Quasiparticle band structures of the polymers and quasiparticle energy levels of the C_{60} molecule are shown in Fig. 2. The corresponding E_v, E_c, and E_g values are listed in Table I under the "G_0W_0" heading. Examining Fig. 2 one finds that the VBM and CBM occur at the Γ point for PT but at the X point for other polymers. These polymers have more structural groups in the unit cell than PT, hence, the band structure is folded at different points in reciprocal space. Macroscopic absorption spectra (χ_2) of the polymers and the C_{60} molecule are shown in Fig. 3. These are defined by $\chi_2 = A\omega\epsilon_2$ for polymers and $\chi_2 = V\omega\epsilon_2$ for the C_{60} molecule where ϵ_2 is the imaginary part of the macroscopic dielectric function, ω is the photon energy, A and V are the cross-sectional area and the volume of the supercell. One can compare various contributions to χ_2 looking at different curves in Fig. 3. Short-dashed blue curves show the joint density of quasiparticle states, long-dashed green curves include the optical transition matrix elements (within the RPA), and solid red curves add the excitonic effects. Optical excitation energies (E_o) corresponding to the peaks of the solid red curves in Fig. 3 and the exciton binding energies ($E_b = E_g - E_o$) are listed in Table I under the "BSE" heading. Note that for the C_{60} molecule, the lowest peak of the short-dashed blue curve at 4.56 eV has no matching peak in the long-dashed green curve. The HOMO–LUMO optical transition in the C_{60} molecule is therefore prohibited by symmetry, in agreement with the previous findings [35]. This implies that the lowest peak of the solid red curve at $E_o = 3.50$ eV originates from optical transitions at higher energies than the HOMO–LUMO gap of $E_g = 4.56$ eV.

All these calculations were performed without taking into account lattice relaxation around charge carriers (polaronic effects). Previous theoretical studies suggest that the polaronic distortion in PT raises E_v by no more than 0.04 eV and lowers E_c by no more than 0.04 eV [36]. These corrections are small and will be neglected in our work, although they could increase due to disorder reducing the effective conjugation length of the PT polymer. Previous experimental studies show that the polaronic distortion in PT lowers E_o by 0.2 eV (the Stokes shift) [37]. According to the Franck-Condon principle, this correction only applies to the photoluminescence process and not to the optical absorption process [37]. Since the photoluminescence process is not relevant for photovoltaic applications, the polaronic correction to E_o will be ignored for

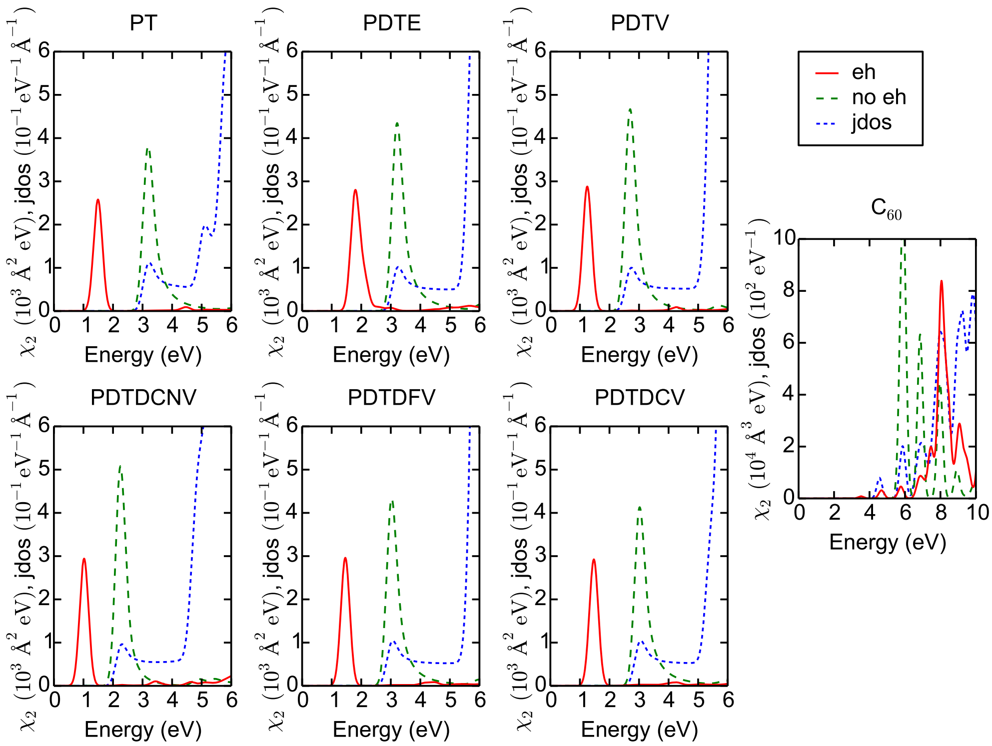

FIG. 3. (Color online) Optical absorption spectra of isolated thiophene-based polymers and isolated C_{60} molecule calculated by solving the Bethe-Salpeter equation (BSE) within the Tamm-Dancoff approximation (decoupling resonant and antiresonant transitions). Chemical names and abbreviations are listed in the first two columns of Table I. Solid red, long-dashed green, and short-dashed blue curves show macroscopic absorption spectra (χ_2) computed with and without electron-hole interaction and the joint density of quasiparticle states (jdos), respectively.

the purpose of our study. Similar corrections are expected in other polymers. The effects of polaronic corrections will be further discussed in Sec. IV.

It is instructive to compare the numbers summarized in Table I with the results of other theoretical and experimental studies from the literature. Previous self-consistent GW and BSE calculations for the isolated PT polymer produced somewhat different results: $E_g = 3.59$ eV, $E_o = 1.74$ eV, and $E_b = 1.85$ eV [38]. It is known that different self-consistent GW schemes generally yield larger band gaps as compared to the G_0W_0 method employed in this work [39–44]. To validate our calculations, we performed eigenvalue self-consistent GW calculation for isolated PT polymer, and we obtained $E_v = -5.75$ eV, $E_c = -2.18$ eV, and $E_g = 3.57$ eV, in good agreement with the literature value of $E_g = 3.59$ eV [38]. Recent G_0W_0 calculation for the isolated C_{60} molecule gave $E_v = -7.28$ eV, $E_c = -2.84$ eV, and $E_g = 4.44$ eV [45], which is close to our numbers from Table I. Similarly to the

TABLE II. Photoelectron spectroscopy (PES), optical absorption (OA), and spectroscopic ellipsometry (SE) measurements on P3HT polymer, C_{60} and PCBM molecules in solid and gas phases from the literature. The meanings of E_v, E_c, E_g, E_o, and E_b are the same as in Table I. All energies are in eV.

Abbreviations and chemical names		Phase	Technique	E_v	E_c	E_g	E_o	E_b
P3HT	poly(3-hexylthiophene)	Solid	PES + OA[a]			2.60	1.85	0.75
P3HT	poly(3-hexylthiophene)	Solid	PES[b]	−4.65	−2.13	2.52		
C_{60}	buckminsterfullerene	Gas	PES[c]	−7.59	−2.69	4.90		
C_{60}	buckminsterfullerene	Solid	SE[d]			2.30		
PCBM	[6,6]-phenyl-C_{61} butyric acid methyl ester	Gas	PES[e]	−7.17				
PCBM	[6,6]-phenyl-C_{61} butyric acid methyl ester	Solid	PES[f]	−5.80	−3.80	2.00		
PCBM	[6,6]-phenyl-C_{61} butyric acid methyl ester	Solid	PES[g]	−5.96	−3.90	2.06		

[a]From Ref. [46].
[b]From Ref. [47].
[c]From Refs. [48,49].
[d]From Ref. [50].
[e]From Ref. [51].
[f]From Ref. [47].
[g]From Ref. [51].

case of PT, self-consistent GW calculation for the isolated C_{60} molecule resulted in a slightly larger band gap: $E_v = -7.41$ eV, $E_c = -2.50$ eV, and $E_g = 4.91$ eV [45]. These numbers agree well with the results of photoelectron spectroscopy (PES) measurements on the C_{60} molecule in gas phase listed in Table II. More comparison with experiment will be done in Sec. III where the effects of environment are taken into account.

III. ENVIRONMENTAL EFFECTS

Aqueous solubility of polymers is achieved through replacing the hydrogen atoms on polymer backbones with alkyl or alkoxy functional groups, known as side chain substitution. Similarly, various functional groups can be covalently bonded to the C_{60} molecule. When these materials are blended together, electrostatic dipole layers are formed at numerous interfaces between the polymers and C_{60} molecules due to spontaneous charge transfer. Furthermore, the electronic orbitals of adjacent C_{60} molecules in the nanocrystalline domains strongly overlap or hybridize. Hybridization between the electronic orbitals of adjacent polymer backbones, although significant in crystalline unsubstituted polymers, is expected to be weak in the case of side chain substitution [52]. Finally, the Coulomb interaction between charge carriers is screened by polarization of the surrounding polymers and molecules. In this section, we explore the question as to what extent the electronic and optical properties of thiophene-based polymers and C_{60} molecule are altered by the side chain substitution, the interface dipole layer, the hybridization of electronic orbitals, and the polarization of the BHJ blend.

To study the effects of side chain substitution, we picked PT and PDTV polymers substituted with methyl and hexyl side groups in regioregular head-to-tail positions (PMeT, P3HT, and P3HDTV) and 1,2-methanofullerene C_{60} molecule substituted with phenyl and butyric acid methyl ester side groups (PCBM). Chemical names and abbreviations of these substances are listed in the first two columns of Table I, and their ball-and-stick models are shown in Fig. 4. We performed DFT/G_0W_0/BSE calculations for methyl-substituted PT polymer (PMeT), while only DFT calculations were carried out for hexyl-substituted PT and PDTV polymers (P3HT and P3HDTV) and substituted 1,2-methanofullerene C_{60} molecule (PCBM) due to the high computational cost of G_0W_0 and BSE steps for these systems. The computational details are the same as outlined in Sec. II. The results of our calculations are summarized in Table I. Comparing the G_0W_0 band edges for PT and PMeT in Table I suggests that methyl substitution shifts the VBM and CBM upwards by 0.37 and 0.28 eV, respectively. It is interesting to note that DFT gives similar values for the shifts in VBM and CBM, namely, 0.32 and 0.34 eV. These shifts in energy levels are induced by electron donation from side groups to the polymer backbone [51]. We conclude that this process is reliably described at the DFT level. Within the DFT, hexyl substitution is found to increase the shifts in energy levels compared to methyl substitution, to 0.47 eV for the VBM and 0.41 eV for the CBM. In the case of PDTV, the energy levels are shifted by 0.38 eV for the VBM and 0.24 eV for the CBM, suggesting that the energy shifts are not very sensitive to changing the polymer backbone. Similarly,

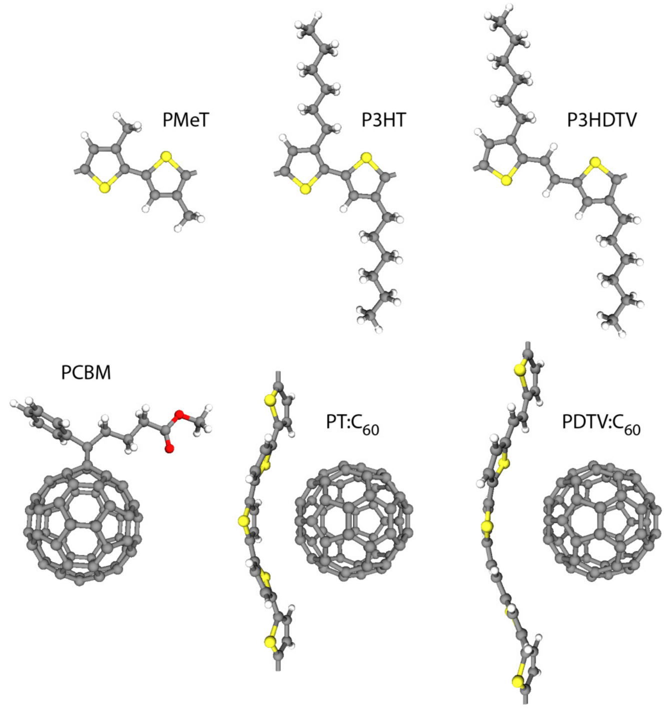

FIG. 4. (Color online) Ball-and-stick models of PT and PDTV polymers substituted with methyl and hexyl side groups in regioregular head-to-tail positions (PMeT, P3HT, and P3HDTV), 1,2-methanofullerene C_{60} molecule substituted with phenyl and butyric acid methyl ester side groups (PCBM), PT:C_{60} and PDTV:C_{60} interfaces. Chemical names and abbreviations are listed in the first two columns of Table II. White, gray, red, and yellow spheres represent hydrogen, carbon, oxygen, and sulfur atoms, respectively.

DFT predicts that the HOMO and LUMO levels of PCBM are shifted upward from the ones of C_{60} by 0.41 and 0.23 eV, respectively. This prediction is in good agreement with the 0.42-eV shift of the HOMO level obtained from photoelectron spectroscopy data for C_{60} and PCBM in gas phase shown in Table II.

Changes to the band edges induced by the formation of the dipole layer were investigated by modeling the interfaces between PT and PDTV polymers and C_{60} molecule within the DFT. Atomic positions were relaxed to equilibrium using the local density approximation (LDA) [53] for the exchange-correlation potential. Ball-and-stick models of the interfaces are shown in Fig. 4. The shortest distance between the atoms in PT and C_{60} was found to be 3.25 Å. Table I shows the band edges of the interfaces computed using the PBE exchange-correlation functional [20,21]. Analysis of the DFT Kohn-Sham orbitals showed that the VBM and CBM of the PT:C_{60} interface originate from the VBM of PT and the LUMO of C_{60}, respectively. The former is shifted downward by 0.23 eV and the latter is shifted upward by 0.13 eV as can be seen by comparing the DFT band edges of PT, C_{60}, and PT:C_{60} in Table I. In case of PDTV, we get similar values for the energy shifts, respectively 0.18 and 0.11 eV, suggesting that the dipole layer is insensitive to the polymer backbone. The total-energy barrier at the PT:C_{60} interface sums up to 0.36 eV. This value is consistent with the dipole barrier of 0.5–0.6 eV at the P3HT:PCBM interface determined by photoemission spectroscopy measurements [47]. This suggests that the interface dipole is satisfactory described within DFT.

Hybridization between the electronic orbitals of adjacent C_{60} molecules broadens the HOMO and LUMO levels into energy bands. The widths of the HOMO and LUMO bands in solid C_{60} are 0.9 and 0.7 eV, respectively, according to G_0W_0 calculations [54]. This implies that E_v and E_c of the isolated C_{60} molecule are corrected approximately by 0.9/2 and −0.7/2 eV, respectively. Hybridization between the electronic orbitals of adjacent polymers is neglected as discussed above.

The polarization of the polymer-molecule blend was modeled as a homogeneous dielectric medium with a spherical cavity surrounding a polymer or a molecule. Such medium is described by the static dielectric matrix [55]

$$\epsilon_{\mathbf{GG}'}(\mathbf{q}) = \delta_{\mathbf{GG}'}\left[1 + \frac{1}{(\epsilon-1)^{-1} + \lambda^2|\mathbf{q}+\mathbf{G}|^2}\right], \quad (1)$$

where $\mathbf{q}$ is a wave vector in the first Brillouin zone, $\mathbf{G}$ and $\mathbf{G}'$ are reciprocal lattice vectors, ϵ is the long-wavelength static dielectric constant of the medium, λ is the mean distance between polymers and molecules, and local fields ($\mathbf{G} \neq \mathbf{G}'$) are neglected. Ellipsometry measurements on P3HT films [56] yielded $\epsilon = 1.70$ and on C_{60} films [50] $\epsilon = 3.61$. X-ray diffraction (XRD) and transition electron microscopy (TEM) diffraction patterns of the crystalline phase of P3HT showed d spacings of 1.61 and 0.38 nm normal and parallel to the sample surface, respectively [16]. Nuclear magnetic resonance (NMR) spectroscopy of nanocrystalline PCBM domains showed the shortest center-to-center distance of 0.98 nm [57]. From these values we deduced $\lambda = 0.83$ nm for P3HT and $\lambda = 0.98$ nm for PCBM assuming a close-packed arrangement of P3HT polymers and PCBM molecules.

G_0W_0 and BSE calculations were carried out for thiophene-based polymers and C_{60} molecule embedded in the dielectric medium described by Eq. (1) taking the values of ϵ and λ for P3HT and PCBM, respectively. Contributions to the electron self-energy from the dielectric medium were computed in the static Coulomb-hole-plus-screened-exchange (COHSEX) approximation (the static limit of GW) and added to the quasiparticle energies of isolated polymers and isolated C_{60} molecule from Sec. II. The direct term of the BSE Hamiltonian was obtained by summing the statically screened Coulomb interaction in isolated polymers and the isolated C_{60} molecule from Sec. II with the one computed from Eq. (1). The results of these calculations are summarized in Table III. For the C_{60} molecule, we find that $E_o = 3.43$ eV is larger than $E_g = 3.15$ eV, meaning that the lowest exciton becomes resonant. Therefore, E_o and E_b are omitted in the last row of Table III. Comparing the values in Tables I and III, we conclude that polarization of the environment reduces both quasiparticle band gaps E_g and exciton binding energies E_b while optical excitation energies E_o remain largely unaffected, a trend that is similar to what has been seen in other nanomaterials such as carbon nanotubes.

Let us compare the results for PT and C_{60} from Table III with the available experimental data for P3HT, C_{60}, and PCBM films summarized in Table II. First, the side chain corrections determined earlier within DFT are applied to E_v and E_c values from Table III. Second, the hybridization corrections extracted from G_0W_0 calculations are applied to E_v and E_c of C_{60}. This gives the corrected band edges

$$\begin{aligned} E_v^d &= -4.93 + 0.47 = -4.46 \text{ eV},\\ E_c^d &= -2.72 + 0.41 = -2.31 \text{ eV},\\ E_v^a &= -6.61 + 0.41 + 0.9/2 = -5.75 \text{ eV},\\ E_c^a &= -3.46 + 0.23 - 0.7/2 = -3.58 \text{ eV}, \end{aligned} \quad (2)$$

where d and a superscripts stand for electron donor (PT) and electron acceptor (C_{60}), respectively. These values are within 0.2 eV of experimental numbers listed in Table II. Quasiparticle band gaps $E_g = E_c - E_v$ and optical excitation energies E_o shown in Table III deviate from experimental values in Table II by 0.4 eV for PT and by 0.2 eV for C_{60}. The larger discrepancy for PT compared to C_{60} may indicate that the spherical cavity model given by Eq. (1) is less accurate for polymers than for molecules.

IV. INTERFACE ENERGETICS

Using the results of Sec. III, we proceed with computing the band offsets at the interface between thiophene-based polymers and the C_{60} molecule. For PT and PDTV, we apply the side chain corrections and the interface dipole corrections determined within DFT in Sec. III. An average of PT and PDTV corrections is used for the remaining polymers. This introduces errors in E_v^d and E_c^a of about 0.04 and 0.02 eV, respectively, according to the values of the corrections listed in Sec. III. Furthermore, we assume that the side chain substitution and the interface dipole layer do not affect E_o. The corrected band edges for PT and C_{60} are computed by

TABLE III. Results of the G_0W_0 + COHSEX and BSE calculations for thiophene-based polymers and the C_{60} molecule in a dielectric medium. Parameters ϵ and λ entering Eq. (1) are listed for different types of dielectric media. The meanings of E_v, E_c, E_g, E_o, and E_b are the same as in Table I. All energies are in eV, λ is in nm.

Abbreviations and chemical names		Medium	ϵ	λ	E_v	E_c	E_g	E_o	E_b
PT	polythiophene	P3HT	1.70	0.83	−4.93	−2.72	2.21	1.39	0.82
PDTE	poly(dithiophene ethyne)	P3HT	1.70	0.83	−5.12	−2.85	2.27	1.59	0.68
PDTV	poly(dithiophene vinylene)	P3HT	1.70	0.83	−4.76	−2.96	1.80	1.11	0.69
PDTDCNV	poly(dithiophene dicyanovinylene)	P3HT	1.70	0.83	−5.69	−4.26	1.43	0.84	0.59
PDTDFV	poly(dithiophene difluorovinylene)	P3HT	1.70	0.83	−5.08	−2.99	2.09	1.33	0.76
PDTDCV	poly(dithiophene dichlorovinylene)	P3HT	1.70	0.83	−5.18	−3.09	2.08	1.34	0.74
C_{60}	buckminsterfullerene	PCBM	3.61	0.98	−6.61	−3.46	3.15		

TABLE IV. Results of the G_0W_0 + COHSEX and BSE calculations for the interface between thiophene-based polymers and C_{60} molecule. E_o is the optical excitation energy from Table III. ΔE_f is the splitting of the quasi-Fermi levels at the interface given by Eq. (4). All energies are in eV.

Abbreviations and chemical names		E_o	ΔE_f
PT	polythiophene	1.39	1.24
PDTE	poly(dithiophene ethyne)	1.59	1.44
PDTV	poly(dithiophene vinylene)	1.11	1.09
PDTDCNV	poly(dithiophene dicyanovinylene)	0.84	2.00
PDTDFV	poly(dithiophene difluorovinylene)	1.33	1.40
PDTDCV	poly(dithiophene dichlorovinylene)	1.34	1.49

adding the interface dipole corrections to Eq. (2):

$$\begin{aligned} E_v^d &= -4.93 + 0.47 - 0.23 = -4.69 \text{ eV}, \\ E_c^d &= -2.72 + 0.41 - 0.23 = -2.54 \text{ eV}, \\ E_v^a &= -6.61 + 0.41 + 0.9/2 + 0.13 = -5.62 \text{ eV}, \\ E_c^a &= -3.46 + 0.23 - 0.7/2 + 0.13 = -3.45 \text{ eV}. \end{aligned} \tag{3}$$

The splitting of the quasi-Fermi levels at the PT:C_{60} interface is given by

$$\Delta E_f = E_c^a - E_v^d = 1.24 \text{ eV}. \tag{4}$$

This is the formation energy of a separated electron-hole pair with an electron on the C_{60} molecule and a hole on the PT polymer. This is to be compared with $E_o = 1.39$ eV from the first line of Table III which represents the formation energy of an electron-hole pair on the PT polymer. The resulting values of E_o and ΔE_f for PT and other polymers are summarized in Table IV.

The optimal value of E_o which minimizes energy losses in the absorption of solar radiation is 1.31 eV [19]. Charge separation at the interface with the C_{60} molecule occurs if $\Delta E_f < E_o$, with $E_o - \Delta E_f$ being the energy loss during charge separation and ΔE_f setting the maximum achievable open circuit voltage. In principle, polaronic corrections need to be applied to the charge separation condition but not to the optical absorption condition. The polaronic distortion lowers ΔE_f by 0.04 eV according to the numbers given in Sec. II (because it raises E_v^d by 0.04 eV and the E_c^a is unaffected). According to the Franck-Condon principle energy diagram, the photogenerated exciton loses roughly half the Stokes shift (0.1 eV) to the lattice before it diffuses to the interface where it breaks up. This implies that the energy loss at the interface (which is the absorption energy minus half the Stokes shift minus ΔE_f) is lowered by 0.06 eV, and the maximum achievable open circuit voltage ΔE_f is lowered by 0.04 eV by the polaronic effect in the polymer. These corrections are much smaller than 0.2–0.4 eV differences between the calculated and measured energy levels, and therefore can be neglected in the present analysis. We thus conclude that the optimal performance is achieved when $E_o = \Delta E_f = 1.31$ eV.

Looking at the numbers in Table IV, we find that using PDTE moves E_o further away from the optimal value as compared to PT. On the other hand, switching to PDTV brings both E_o and ΔE_f to nearly optimal values, especially considering that the G_0W_0 method underestimates both E_o and ΔE_f (gives lower E_c^a and higher E_v^d) as compared to self-consistent GW schemes (see discussion in Sec. II). Moving to PDTDCNV slightly lowers E_o but substantially raises ΔE_f due to the strong electron acceptor character of the cyanovinylene unit. This prevents the charge separation from occurring at the interface. Substituting cyano groups with halogens (fluorine in PDTDFV or chlorine in PDTDCV) restores E_o of PT and brings ΔE_f to the values slightly larger than E_o. Overall, we conclude that replacing PT with PDTV minimizes energy losses during both optical absorption and charge separation processes. We limit our analysis to this qualitative assessment and do not attempt to estimate the energy conversion efficiency of PDTV-based BHJ solar cells. The latter will be affected by many factors in addition to the interface energetics as noted in Sec. I.

V. SUMMARY

In summary, we computed the quasiparticle and optical spectra of several different thiophene-, ethyne-, and vinylene-based copolymers and fullerene derivatives using the GW method and the GW plus Bethe-Salpeter equation approach based on the many-body Green's function theory. The effects of side chain substitution, formation of the interface dipole layer, hybridization of electronic orbitals, and polarization of the bulk heterojunction blend are taken into account in an approximate way. The quasiparticle and optical spectra corrected for these environmental effects show a quantitative agreement with the available experimental data. One of the polymers studied in this work, poly(dithiophene vinylene), is predicted to reduce the losses in photovoltaic energy conversion as compared to polythiophene-based bulk heterojunction solar cells. Other polymers studied here are predicted to perform worse than polythiophene.

ACKNOWLEDGMENTS

The authors acknowledge helpful discussions with Professor Michel Côté and Professor Jeffrey C. Grossman. This research was supported by the sp2 Program at the Lawrence Berkeley National Laboratory through the Office of Basic Energy Sciences, U. S. Department of Energy under Contract No. DE-AC02-05CH11231 which provided for the excited-state GW and GW-BSE calculations and simulations, and by the National Science Foundation under Grant No. DMR10-1006184 which provided for the structural determination and interfacial studies. S.G.L. acknowledges support of a Simons Foundation Fellowship in Theoretical Physics. Computational resources have been provided by NSF through TeraGrid resources at NICS and by DOE at Lawrence Berkeley National Laboratory's NERSC facility.

[1] H. Spanggaard and F. C. Krebs, Sol. Energy Mater. Sol. Cells **83**, 125 (2004).

[2] M. Reyes-Reyes, K. Kim, and D. L. Carroll, Appl. Phys. Lett. **87**, 083506 (2005).

[3] G. Li, V. Shrotriya, J. Huang, Y. Yao, T. Moriarty, K. Emery, and Y. Yang, Nat. Mater. **4**, 864 (2005).

[4] W. Ma, C. Yang, X. Gong, K. Lee, and A. J. Heeger, Adv. Funct. Mater. **15**, 1617 (2005).

[5] Y. Kim, S. Cook, S. M. Tuladhar, S. A. Choulis, J. Nelson, J. R. Durrant, D. D. C. Bradley, M. Giles, I. McCulloch, C.-S. Ha, and M. Ree, Nat. Mater. **5**, 197 (2006).
[6] K. Kim, J. Liu, M. A. G. Namboothiry, and D. L. Carroll, Appl. Phys. Lett. **90**, 163511 (2007).
[7] M. C. Scharber, D. Mühlbacher, M. Koppe, P. Denk, C. Waldauf, A. J. Heeger, and C. J. Brabec, Adv. Mater. **18**, 789 (2006).
[8] L. J. A. Koster, V. D. Mihailetchi, and P. W. M. Blom, Appl. Phys. Lett. **88**, 093511 (2006).
[9] R. A. J. Janssen and J. Nelson, Adv. Mater. **25**, 1847 (2013).
[10] H.-Y. Chen, J. Hou, S. Zhang, Y. Liang, G. Yang, Y. Yang, L. Yu, Y. Wu, and G. Li, Nat. Photonics **3**, 649 (2009).
[11] Y. Liang, Z. Xu, J. Xia, S.-T. Tsai, Y. Wu, G. Li, C. Ray, and L. Yu, Adv. Mater. **22**, E135 (2010).
[12] Z. He, C. Zhong, X. Huang, W.-Y. Wong, H. Wu, L. Chen, S. Su, and Y. Cao, Adv. Mater. **23**, 4636 (2011).
[13] C. E. Small, S. Chen, J. Subbiah, C. M. Amb, S.-W. Tsang, T.-H. Lai, J. R. Reynolds, and F. So, Nat. Photonics **6**, 115 (2012).
[14] Z. He, C. Zhong, S. Su, M. Xu, H. Wu, and Y. Cao, Nat. Photonics **6**, 591 (2012).
[15] J. You, L. Dou, K. Yoshimura, T. Kato, K. Ohya, T. Moriarty, K. Emery, C.-C. Chen, J. Gao, G. Li, and Y. Yang, Nat. Commun. **4**, 1446 (2013).
[16] P. Vanlaeke, A. Swinnen, I. Haeldermans, G. Vanhoyland, T. Aernouts, D. Cheyns, C. Deibel, J. D'Haen, P. Heremans, J. Poortmans, and J. Manca, Sol. Energy Mater. Sol. Cells **90**, 2150 (2006).
[17] J. Guo, H. Ohkita, H. Benten, and S. Ito, J. Am. Chem. Soc. **132**, 6154 (2010).
[18] J. M. Szarko, J. Guo, B. S. Rolczynski, and L. X. Chen, J. Mater. Chem. **21**, 7849 (2011).
[19] L. C. Hirst and N. J. Ekins-Daukes, Prog. Photovoltaics **19**, 286 (2011).
[20] J. P. Perdew, K. Burke, and M. Ernzerhof, Phys. Rev. Lett. **77**, 3865 (1996).
[21] J. P. Perdew, K. Burke, and M. Ernzerhof, Phys. Rev. Lett. **78**, 1396 (1997).
[22] N. Troullier and J. L. Martins, Phys. Rev. B **43**, 1993 (1991).
[23] L. Kleinman and D. M. Bylander, Phys. Rev. Lett. **48**, 1425 (1982).
[24] L. Hedin and S. Lundqvist, in *Advances in Research and Applications*, Solid State Physics, Vol. 23, edited by F. Seitz, D. Turnbull, and H. Ehrenreich (Academic, New York, 1970), pp. 1–181.
[25] M. S. Hybertsen and S. G. Louie, Phys. Rev. B **34**, 5390 (1986).
[26] G. Strinati, Riv. Nuovo Cimento **11**, 1 (1988).
[27] M. Rohlfing and S. G. Louie, Phys. Rev. B **62**, 4927 (2000).
[28] B. G. Pfrommer, J. Demmel, and H. Simon, J. Comput. Phys. **150**, 287 (1999).
[29] J. Deslippe, G. Samsonidze, D. Strubbe, M. Jain, M. L. Cohen, and S. G. Louie, Comput. Phys. Commun. **183**, 1269 (2012).
[30] M. L. Cohen, M. Schlüter, J. R. Chelikowsky, and S. G. Louie, Phys. Rev. B **12**, 5575 (1975).
[31] S. Ismail-Beigi, Phys. Rev. B **73**, 233103 (2006).
[32] C. A. Rozzi, D. Varsano, A. Marini, E. K. U. Gross, and A. Rubio, Phys. Rev. B **73**, 205119 (2006).
[33] H. J. Monkhorst and J. D. Pack, Phys. Rev. B **13**, 5188 (1976).
[34] J. Deslippe, G. Samsonidze, M. Jain, M. L. Cohen, and S. G. Louie, Phys. Rev. B **87**, 165124 (2013).
[35] G. F. Bertsch, A. Bulgac, D. Tománek, and Y. Wang, Phys. Rev. Lett. **67**, 2690 (1991).
[36] G. Brocks, Synth. Met. **102**, 914 (1999).
[37] K. Sakurai, H. Tachibana, N. Shiga, C. Terakura, M. Matsumoto, and Y. Tokura, Phys. Rev. B **56**, 9552 (1997)..
[38] J.-W. van der Horst, P. A. Bobbert, M. A. J. Michels, G. Brocks, and P. J. Kelly, Phys. Rev. Lett. **83**, 4413 (1999).
[39] M. van Schilfgaarde, T. Kotani, and S. Faleev, Phys. Rev. Lett. **96**, 226402 (2006).
[40] F. Bruneval, N. Vast, and L. Reining, Phys. Rev. B **74**, 045102 (2006).
[41] M. Shishkin and G. Kresse, Phys. Rev. B **75**, 235102 (2007).
[42] F. Fuchs, J. Furthmüller, F. Bechstedt, M. Shishkin, and G. Kresse, Phys. Rev. B **76**, 115109 (2007).
[43] T. Kotani, M. van Schilfgaarde, and S. V. Faleev, Phys. Rev. B **76**, 165106 (2007).
[44] F. Bechstedt, F. Fuchs, and G. Kresse, Phys. Status Solidi B **246**, 1877 (2009).
[45] X. Blase, C. Attaccalite, and V. Olevano, Phys. Rev. B **83**, 115103 (2011).
[46] C. Deibel, D. Mack, J. Gorenflot, A. Schöll, S. Krause, F. Reinert, D. Rauh, and V. Dyakonov, Phys. Rev. B **81**, 085202 (2010).
[47] Z.-L. Guan, J. B. Kim, H. Wang, C. Jaye, D. A. Fischer, Y.-L. Loo, and A. Kahn, Org. Electron. **11**, 1779 (2010).
[48] H. Steger, J. Holzapfel, A. Hielscher, W. Kamke, and I. Hertel, Chem. Phys. Lett. **234**, 455 (1995).
[49] X.-B. Wang, C.-F. Ding, and L.-S. Wang, J. Chem. Phys. **110**, 8217 (1999).
[50] S. L. Ren, Y. Wang, A. M. Rao, E. McRae, J. M. Holden, T. Hager, K. Wang, W.-T. Lee, H. F. Ni, J. Selegue, and P. C. Eklund, Appl. Phys. Lett. **59**, 2678 (1991).
[51] K. Akaike, K. Kanai, H. Yoshida, J. Tsutsumi, T. Nishi, N. Sato, Y. Ouchi, and K. Seki, J. Appl. Phys. **104**, 023710 (2008).
[52] J.-W. van der Horst, P. A. Bobbert, and M. A. J. Michels, Phys. Rev. B **66**, 035206 (2002).
[53] J. P. Perdew and A. Zunger, Phys. Rev. B **23**, 5048 (1981).
[54] E. L. Shirley and S. G. Louie, Phys. Rev. Lett. **71**, 133 (1993).
[55] G. Cappellini, R. Del Sole, L. Reining, and F. Bechstedt, Phys. Rev. B **47**, 9892 (1993).
[56] R. Jansson, H. Arwin, G. Gustafsson, and O. Inganäs, Synth. Met. **28**, 371 (1989).
[57] M. T. Rispens, A. Meetsma, R. Rittberger, C. J. Brabec, N. S. Sariciftci, and J. C. Hummelen, Chem. Commun. **17**, 2116 (2003).